Mon. Not. R. Astron. Soc. **000**, 000–000 (0000) Printed 23 January 1998

A spectropolarimetric survey of northern-hemisphere Wolf-Rayet stars

T.J. Harries[1], D.J. Hillier[2], and I.D. Howarth[3]

[1] *Mullard Space Science Laboratory, University College London, Holmbury St. Mary, Dorking, Surrey RH5 6NT, UK.*
[2] *Department of Physics and Astronomy, University of Pittsburgh, 3941 O'Hara Street, Pittsburgh, PA 15260, U.S.A.*
[3] *Department of Physics and Astronomy, University College London, Gower Street, London WC1E 6BT, UK.*

Dates to be inserted

ABSTRACT

We present a homogeneous, high-signal-to-noise spectropolarimetric survey of 16 northern-hemisphere Wolf-Rayet (WR) stars. A reduction in polarization at emission-line wavelengths – the 'line effect' – is identified in four stars: WRs 134, 137, 139, and 141. The magnitude of the effect in WR 139 (V444 Cyg) is variable, while WR 136, previously reported to show the line effect, does not show it in our data. Assuming the line effect generally to arise from axisymmetric distortions of stellar winds, we show that a model in which all WRs have the same intrinsic (equator-on) polarization, with the observed variation solely due to inclination effects, is inconsistent with the observations. A model in which the intrinsic polarizations are uniformly distributed is more plausible, but best-fit results are obtained if the distribution of polarizations is biased towards small values, with only ∼20% of stars having intrinsic polarizations greater than ∼0.3%. Radiative-transfer calculations indicate that the observed continuum polarizations can be matched by models with equator:pole density ratios of 2–3. The model spectra have electron-scattering wings that are significantly stronger than observed (in both intensity and polarized flux), confirming that the winds of stars showing intrinsic polarization must be clumped on small scales as well as being distorted on large scales.

We combine the results of our survey with observations from the literature to give a sample of 29 stars which have both accurate spectropolarimetric observations and physical parameters derived from standard-model analyses. We find that the line-effect stars are clustered at high $\dot{M}, L$ in the luminosity–mass-loss-rate plane (although they are unexceptional in the terminal velocity–subtype and the surface-mass-flux–temperature planes). The mass-loss rates derived from radio-continuum observations for these stars are in good accord with the results of optical emission-line analyses, suggesting that (i) the wind structure of line-effect stars has a density contrast which is effectively constant with radius, and (ii) the high $\dot{M}$ values may be an artefact of large-scale wind structure. Assuming that observed spectroscopic and photometric variability of the line-effect stars is related to the WR rotation period, we compute equatorial rotation velocities. These velocities correspond to $\sim 10\%$ of the core break-up rates, and may be large enough to produce significant wind-compression effects according to the models of Ignace, Cassinelli & Bjorkman (1996).

Key words: Stars: mass-loss – Stars: early-type – Polarization

1 INTRODUCTION

Wolf-Rayet stars are massive, evolved systems whose characteristic spectra of broad emission lines are produced in dense, high-speed stellar winds. The 'standard model' of Wolf-Rayet stars, which assumes an isotropic, homogeneous, time-independent outflow, is broadly successful in predicting the continuum fluxes and emission-line profiles (e.g., Hillier 1994). However, observational evidence is accumulating that the standard-model assumptions do not provide a complete description of these stars. For example, photopolarimetric continuum variability and time-dependent subpeaks on emission-line profiles suggest small-scale wind structure (e.g., Drissen et al. 1987; Robert et al. 1989; Moffat et al. 1988). There is also growing evidence that the winds of at least some WR stars are anisotropic on larger scales;

for example, a disk-like structure for the WR wind of the WR+O binary system WR 140 has been proposed to explain the periodic variability of its radio emission (White & Becker 1995).

Thomson scattering by free electrons in the winds of WR stars means that gross wind asymmetries, such as disks or oblate-spheroid structures, can be revealed by spectropolarimetric observations. In the spherically symmetric case the polarization from scattered radiation from different regions of the wind cancels, and no nett polarization is observed, but significant linear polarization of the continuum may arise in an asymmetric wind. Since the continuum radiation is formed at smaller radii than the line emission (in a given spectral region), continuum photons 'see' a higher electron-scattering optical depth, τ_{es}. As the polarization is proportional to τ_{es} (in the optically thin limit) the continuum radiation will be more polarized than the line radiation. This leads to the so-called 'line effect', a reduction in observed polarization at emission-line wavelengths which has been observed in several WR stars, notably WR 6 (McLean et al. 1979; Schulte-Ladbeck et al. 1991; Harries et al. 1997) and WR 134 (Schulte-Ladbeck et al. 1992).

The physical cause of departures from spherical symmetry may involve magnetic fields (e.g., Poe, Friend & Cassinelli 1989; Cassinelli 1992) or rapid rotation (see Marchenko 1994). The wind-compression model (Bjorkman & Cassinelli 1993), in which wind material ejected from the 'upper' and 'lower' hemispheres of a rapidly-rotating star converges at the equator, initially appears promising (Ignace, Cassinelli & Bjorkman 1996), although recent results suggest that gravity darkening produces a radiative force *away* from the equator, and that azimuthal radiative forces act against rotation (Owocki, Cranmer & Gayley 1996). These effects combine to impede disk formation; thus, although the observational evidence for global wind asymmetries in some WR stars is well established, the models of wind driving require additional physics.

Are all WR winds asymmetric, with line effects observed only in systems with high inclinations? Or do the line-effect stars represent a distinct subclass where the processes involved in wind driving differ from that of the majority? If so, do the line-effect stars have any identifiable common characteristics? In order to answer these questions we have undertaken linear spectropolarimetry of 16 bright northern-hemisphere WR stars. When the new observations are combined with published results, both reliable spectropolarimetry and physical parameters derived from standard-model analyses are available for a sample of 29 WR stars. We use this sample to try to clarify the properties of line-effect stars.

2 OBSERVATIONS AND DATA REDUCTION

Our targets were chosen simply on the basis of observability (position and brightness), and therefore represent a random sample in terms of polarization properties. Some characteristics of the observed stars are summarized in Table 1.

The observations were made with the ISIS dual-beam Cassegrain spectrograph and polarimetry module on the 4.2-m William Herschel Telescope (WHT) during 1993 July 22–25 (JDs 2449191–4). Only the (mirror-fed) red arm of the spectrograph was used, to avoid low-level 'ghosting' resulting from internal reflection in the dichroic beamsplitter, which can overwhelm weak polarimetry signals. The R316R grating and EEV3 CCD ($1280 \times 1180 \times 22.5\mu$m) gave a mean reciprocal dispersion of 1.38 Å mm^{-1} and a resolution, measured from the widths of arc calibration lines, of approximately 3Å (150 km s^{-1}). All the targets were observed at a central wavelength of 6050Å, with the slit orientation close to the parallactic angle but with the spectrograph rotating (required to maintain constant slit position angle).

A typical observing sequence consisted of a calibration arc exposure followed by four target integrations at the 0°, 45°, 22.5°, and 67.5° positions of the half-wave plate. In addition to the target stars, we obtained data for unpolarized and polarized standard stars, including observations through a nominally 100%-polarizing filter. The frames were debiased using the median bias level in the overscan region, and a mean bias frame subtracted from the images. Cosmic rays were removed from the images by using the BCLEAN routine in the FIGARO data-reduction suite (Shortridge et al. 1996). Polarization spectra were then computed from the images following the algorithm described by Harries & Howarth (1996a). The method includes sky-background subtraction and a first-order compensation for cross-talk between the ordinary (o) and extraordinary (e) spectra. The o and e spectra were wavelength calibrated separately to allow for the small wavelength shift between the two channels introduced by the polarimetry-module optics.

The extracted spectra were transformed to the celestial position-angle system by rotating the Stokes vectors by the slit orientation angle, with a small zero-point correction determined from the polarized standards. The wavelength dependence of the PA, which results from the slight chromatism of the waveplate's fast axis, was removed by using low-order polynomial fits to observations taken through the 100%-polarizing filter. We did not correct for instrumental polarization, which precise observations of an unpolarized standard showed to be less than 0.1%.

The WR polarization spectra, binned to a constant error of 0.05% in P are plotted in Figure 1, and the continuum polarizations are included in Table 1. There is reasonable agreement between our measurements and those presented previously (see Table 1), although it should be noted that the literature values sample rather different wavelength regions (generally b-band) than our observerations.

2.1 Interstellar polarization

All the targets are close to the Galactic plane, and moderately reddened; this results in foreground linear polarization, introduced by interstellar dust grains aligned in the Galactic magnetic field. The magnitude of this interstellar polarization (ISP) scales roughly with the reddening, and may easily exceed the intrinsic polarizations of the targets. It is therefore important to obtain accurate estimates of the ISPs.

Lacking a better alternative, we employ the field-star method to estimate the ISPs of our 16 targets. This method assumes that stars which are close to the target (both along the line of sight and in the plane of the sky) probe the same interstellar material and display the same ISP. Unfortunately, in practice the ISP varies over small angular scales, and alignment of discrete dust clouds along the line of sight

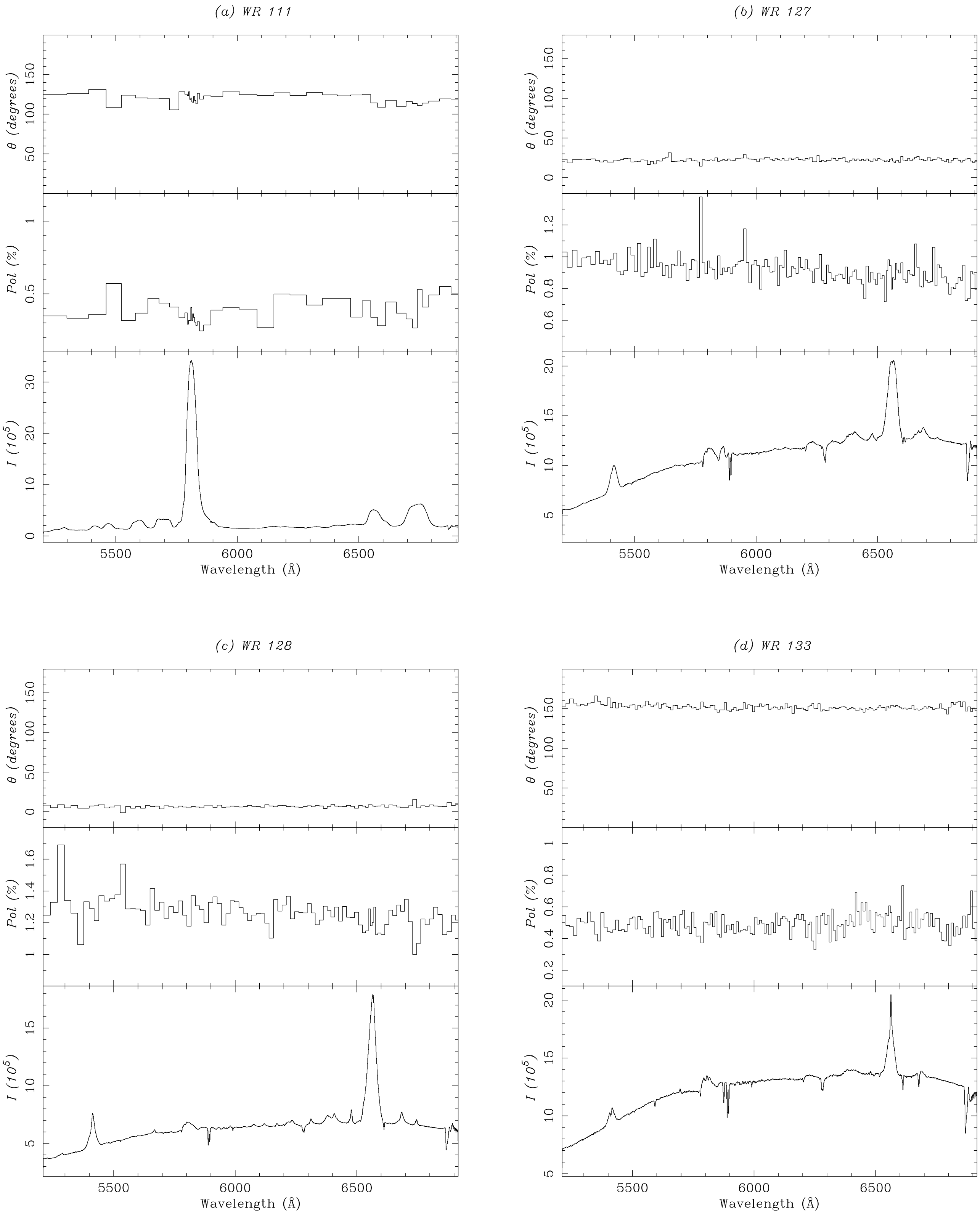

Figure 1. The polarization spectra, binned to a constant error of 0.05% in P. The top section of each panel shows the position angle of the polarization in degrees, the middle panel the percentage polarization, and the bottom panel the (unbinned) intensity spectrum.

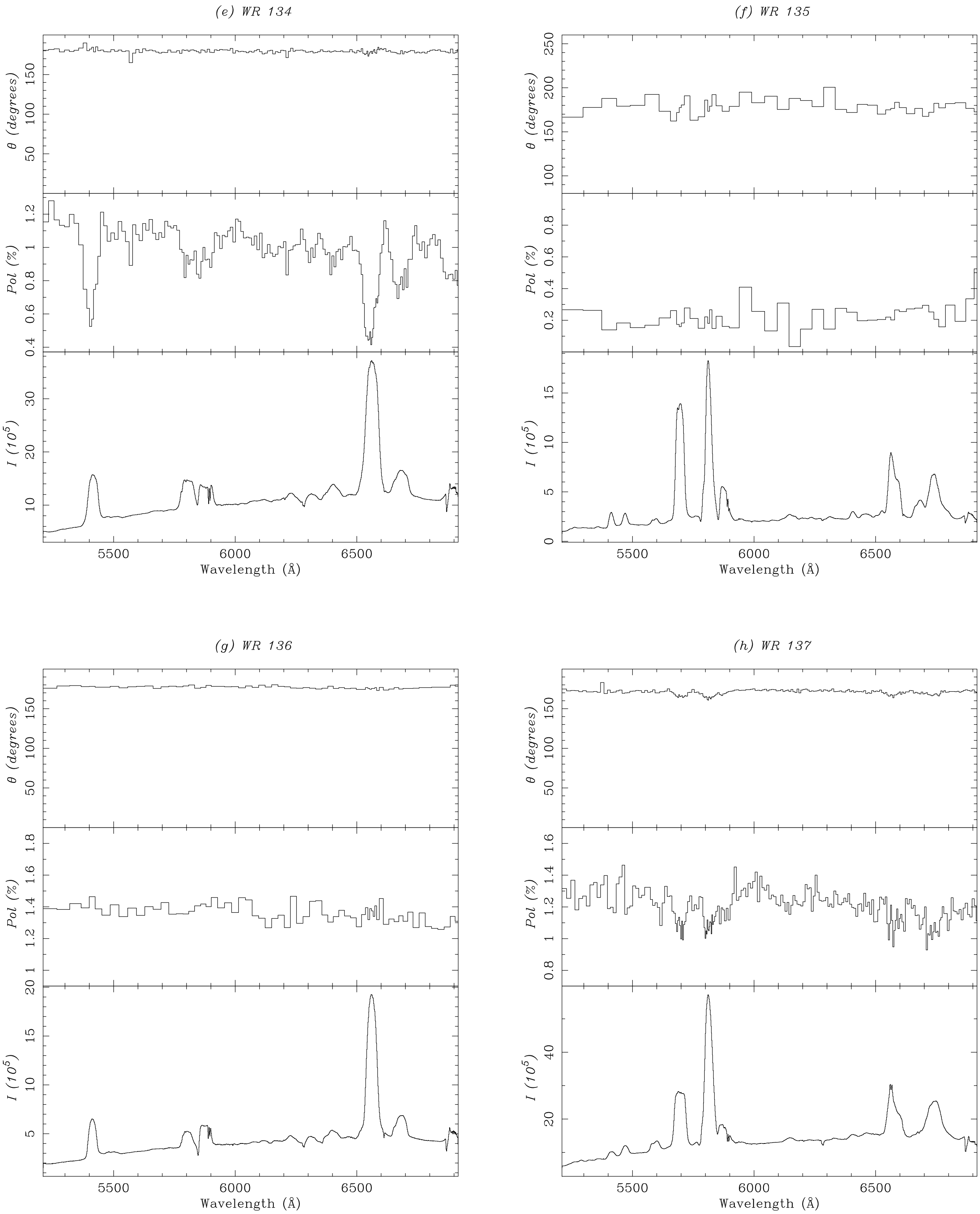

Figure 1. Continued.

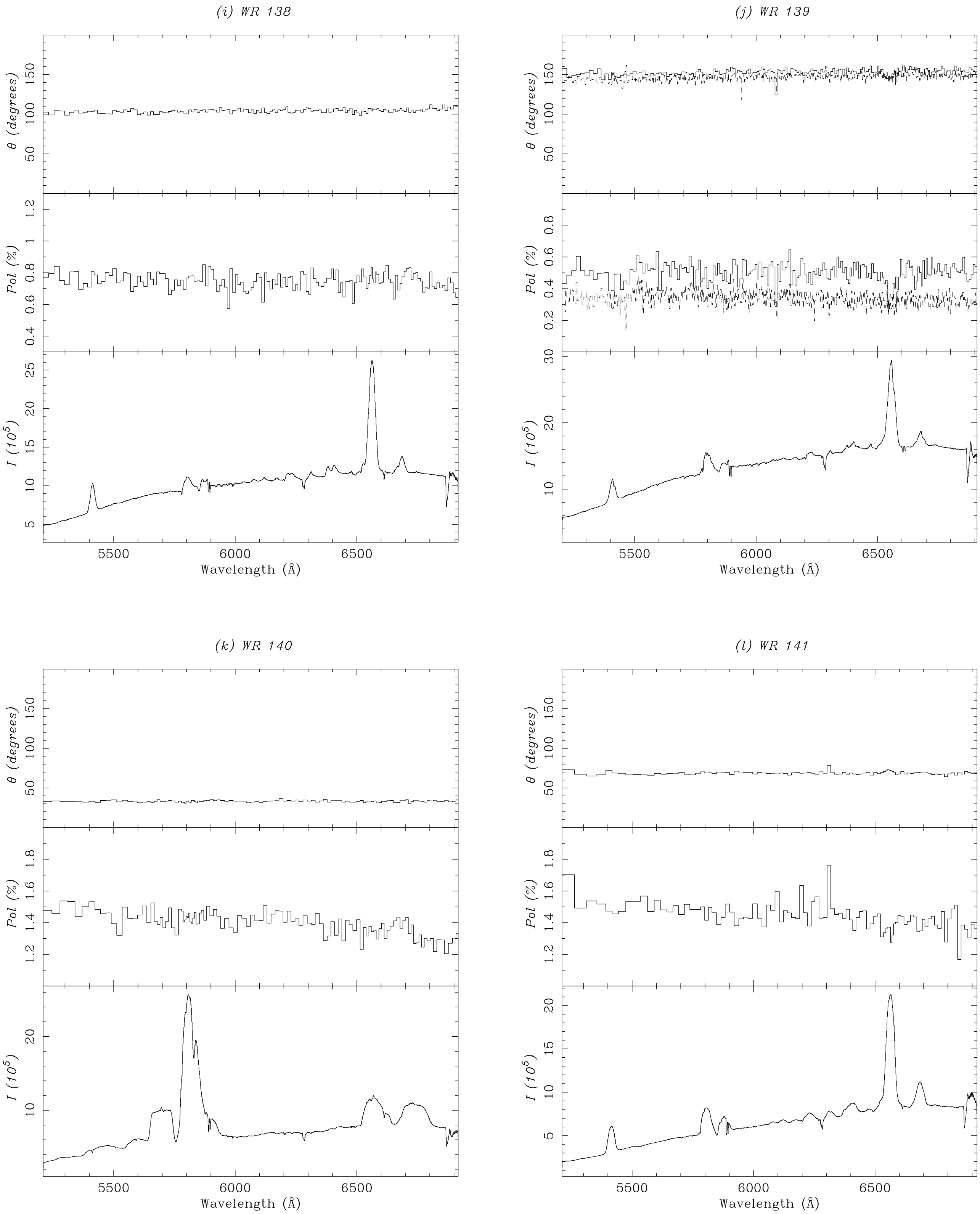

Figure 1. Continued. Two separate polarization spectra of WR 139 are shown.

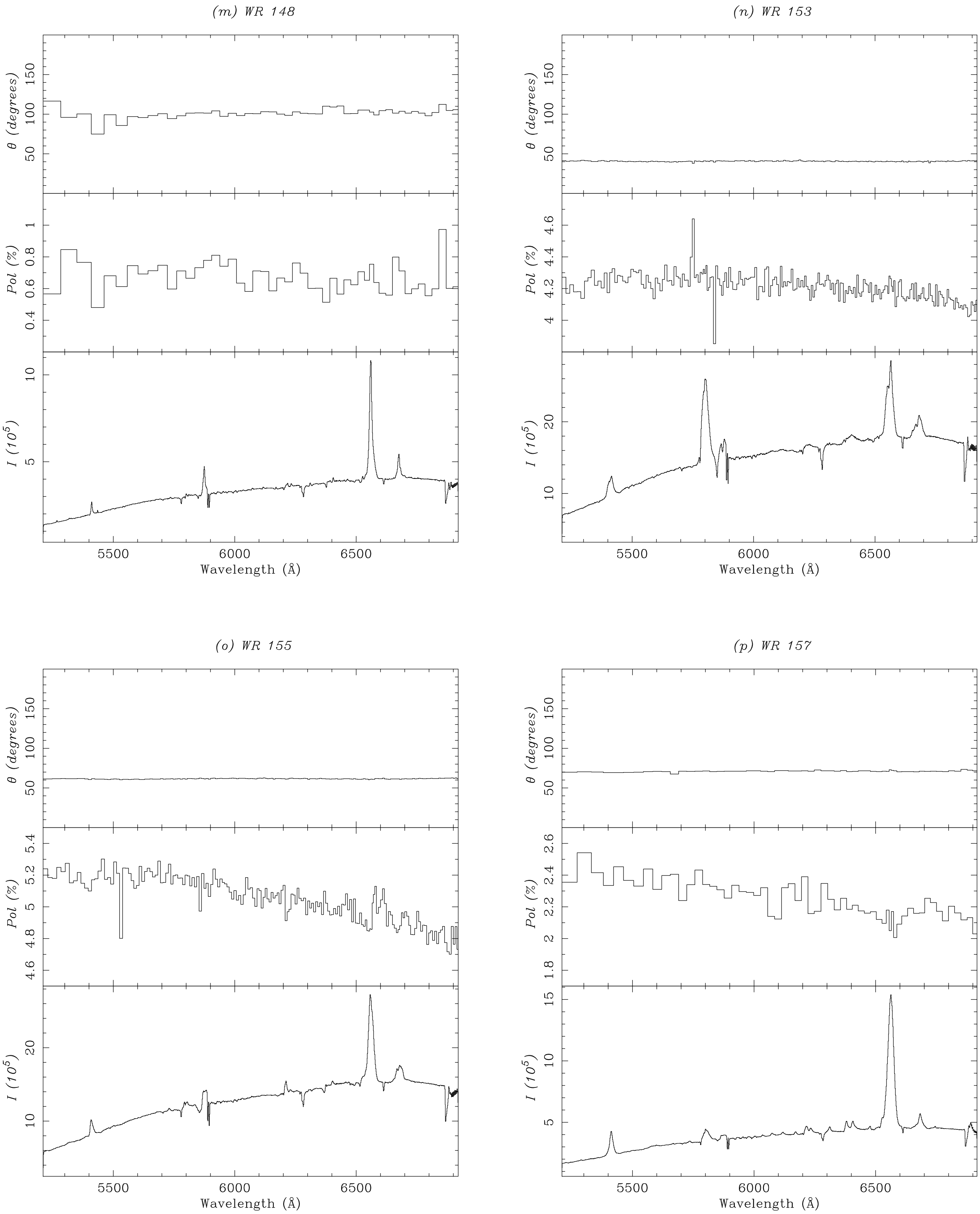

Figure 1. Concluded.

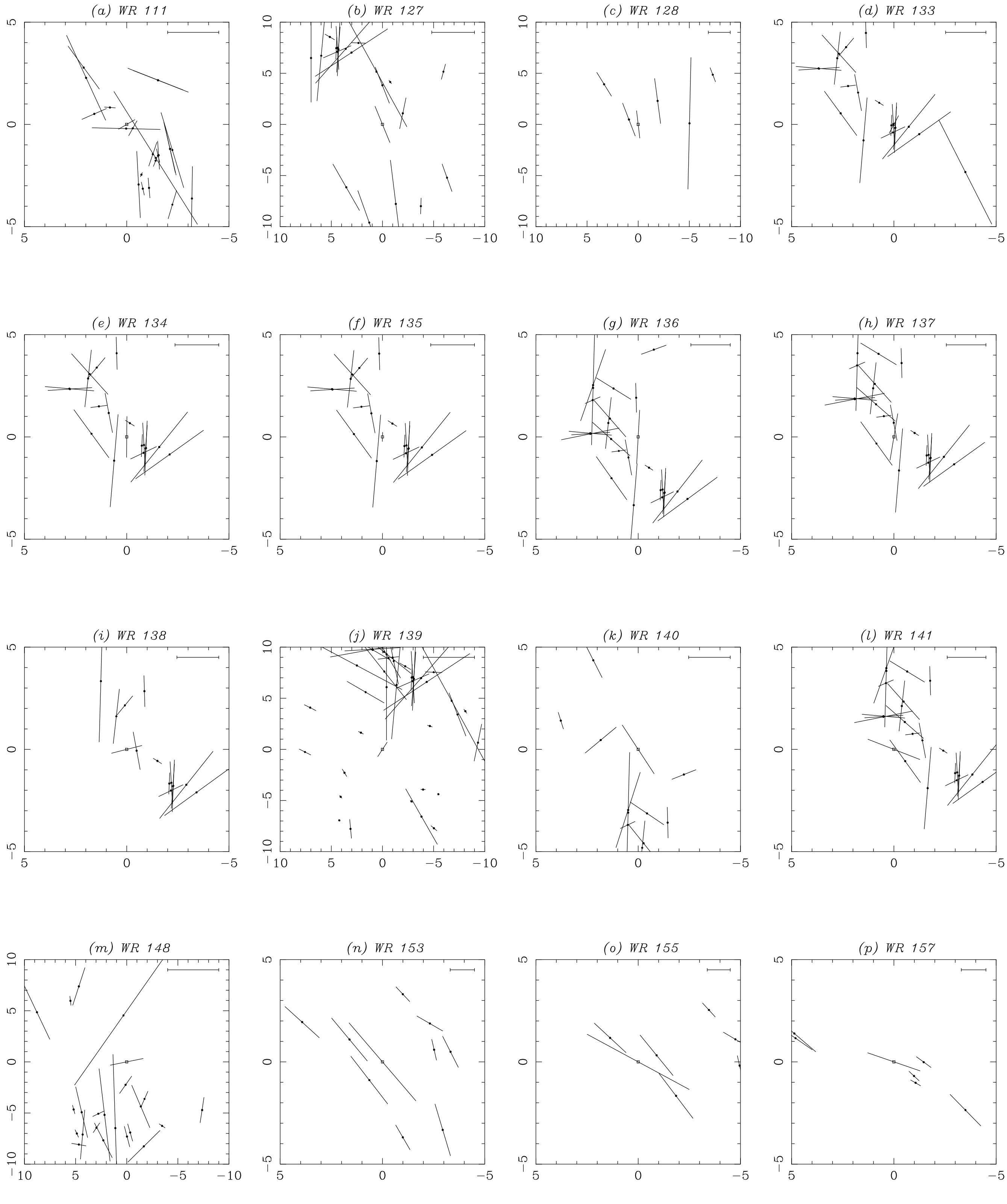

Figure 2. The interstellar-polarization maps around the target stars. The axes are in degrees. The bar at the top right of each figure represents 1% polarization, and the target's continuum polarization is plotted at (0,0).

Table 1. The target list; WR numbers are from the van der Hucht et al. (1988) catalogue, which is also the source for spectral types, and, where relevant, orbital periods. Extinction-free distance moduli, y_0, are from van der Hucht et al. (1988). P_o, θ_o are the observed percentage continuum polarizations and position angles for the target stars, with P_{is}, θ_{is} the median values for N field stars, which we take to be representative of the interstellar polarization (§ 2.1). Previous measurements of the continuum polarization are also given (P_{lit},θ_{lit}); the references are: 1. Robert et al. (1989), 2. St.-Louis et al. 1987, 3. St.-Louis et al. 1988, 4. Drissen et al. (1986) and 5. Harries & Hilditch (1997). [Note that the phase-averaged polarization is given for the binary systems.]

WR	Name	Spec.	$P_{orb}(d)$	P_o	θ_o	P_{is}	θ_{is}	N	y_0	P_{lit}	θ_{lit}	Ref.
111	HD 165763	WC5		0.4 ± 0.1	120 ± 1	0.4	18	22	11.0	0.33	113	2
127	HD 186943	WN4+O9.5V	9.6	0.9 ± 0.1	22 ± 1	0.5	0	21	13.2	1.12	24	3
128	HD 187282	WN4		1.3 ± 0.1	7 ± 1	1.2	13	5	13.0	1.21	9	3
133	HD 190918	WN4.5+O9.5Ib	113	0.5 ± 0.1	152 ± 1	0.2	164	19	11.6	0.47	160	1
134	HD 191765	WN6		0.9 ± 0.1	180 ± 1	0.1	4	18	11.6	0.95	4	1
135	HD 192103	WC8		0.2 ± 0.1	178 ± 1	0.1	4	18	11.6	0.23	8	1
136	HD 192163	WN6	4.5	1.4 ± 0.1	177 ± 1	0.1	111	24	11.3	1.45	178	1
137	HD 192641	WC7	12.6yr[1]	1.2 ± 0.1	171 ± 1	0.1	111	22	11.3	1.18	7.5	1
138	HD 193077	WN5+abs	4yr[4]	0.7 ± 0.1	104 ± 1	0.8	173	13	11.3	0.69	101	1
139*	V444 Cyg	WN5+O6	4.2	0.3 ± 0.1	147 ± 1	0.1	46	39	11.2	0.40	148	1
140	HD 193793	WC7+abs	8yr[3]	1.4 ± 0.1	33 ± 1	0.4	163	11	10.6	1.37	33	1
141	HD 193928	WN6+O5	21.6	1.4 ± 0.1	69 ± 1	0.1	135	23	11.3			
148	HD 197406	WN7	4.3	0.7 ± 0.1	101 ± 1	0.2	20	22	14.4	0.98	107	4
153	GP Cep	WN6/WCE+O	6.7+3.3[2]	4.2 ± 0.1	41 ± 1	1.8	54	9	12.7	4.10	44	3
155	CQ Cep	WN7+O	1.6	5.0 ± 0.1	62 ± 1	1.1	88	6	12.7	5.2	63	5
157	HD 219460	WN4.5+(B1 II)		2.2 ± 0.1	71 ± 1	1.3	92	6	12.8			

*A second observation of WR 139 has $P_o = 0.51 \pm 0.01\%$ at $\theta_o = 153 \pm 0.3°$.
[1] Williams, van der Hucht & Thé (1987).
[2] Panov & Seggewiss (1990).
[3] Williams et al. (1990)
[4] Annuk (1991)

may mean that the magnitude of the ISP does not monotonically increase with distance. Additionally, it is necessary to assume that the field stars are themselves unpolarized, a particularly unsafe assumption for early-type stars which are often polarimetrically active.

Initially, we selected all field stars listed in the polarization catalogues of Mathewson et al. (1978) and Klare & Neckel (1977) within a 5° radius of a given target. For those stars with complete Strömgren photometry in the Hauck & Mermilliod (1990) catalogue, the spectral type and the calibrations given by Crawford (1975, 1978, 1979) were used to estimate the unreddened distance modulus, y_0. For stars with only UBV photometry available (from the catalogue by Mermilliod 1987) we employed the Q method (Heintze 1983) to estimate y_0, with absolute magnitudes from Allen (1973). The distance moduli listed by van der Hucht (1988) were adopted for the target stars. In the majority of cases we included field stars with distance moduli within 2 magnitudes of the target to estimate the ISP. Some targets had no field stars within this volume, and for these systems the tolerance was widened to ±4 magnitudes (WRs 128, 153, and 155), ±6 mags (WRs 127 and 157), or ±8 mags (WRs 139 and 148). In four cases the radius was increased to 10° (WRs 127, 128, 139, and 148). The interstellar polarization maps are plotted in Figure 2.

The ISP patterns about the target stars appear to be rather chaotic (see also Figure 1 of Robert et al. 1989). The region that contains WRs 133–138, in particular, does not show any obvious pattern. As a pragmatic approach, we adopted the medians of the field-star polarization vectors as best estimates of the WR ISP vectors; these are listed in Table 1. Figure 3 shows the ISP plotted as a function of A_V (taken from van der Hucht et al. 1988). Although A_V should be approximately proportional to P_{is} there is only marginal evidence of this in Figure 3.

2.2 Comments on individual stars

WR 111. This WC5 star shows a relatively small continuum polarization, and no evidence for the line effect (Figure 1a), in agreement with Anglo-Australian Telescope observations reported by Schulte-Ladbeck (1994; hereinafter SL94). Photopolarimetric observations show no variability (St.-Louis et al. 1987), suggesting that the observed polarization is primarily interstellar.

WR 127. This WR+O binary showed no measurable line effect at the time of our observation (Figure 1b), in accord with Shane Telescope observations by Schmidt (1988; hereinafter S88). However, intrinsic polarization is revealed by phase-locked variability (St.-Louis et al. 1988).

WR 128. No line effect is observed in this WN4 star (Figure 1c), in agreement with S88. The ISP map suggests that the observed polarization is mostly interstellar in origin (Figure 2c), but photopolarimetric observations of the system reveal low-amplitude variations (St.-Louis et al. 1988).

WR 133. A WN4.5+O binary star; we observe no line effect (Figure 1d), in agreement with S88. The ISP map shows

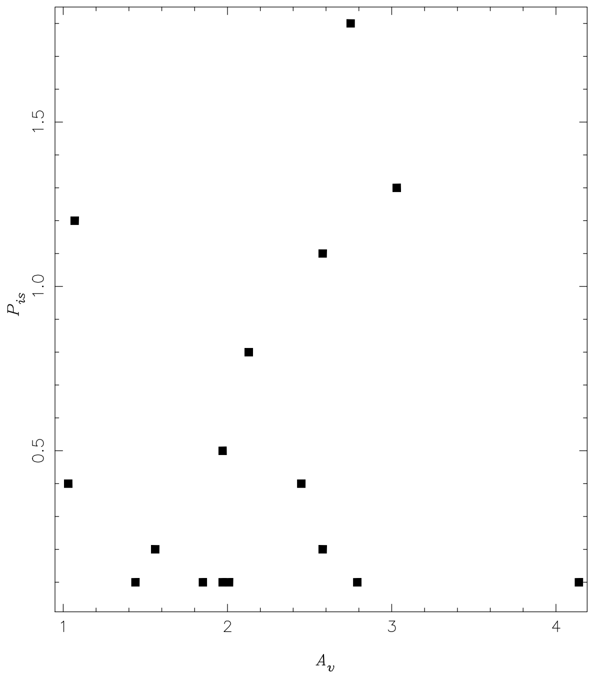

Figure 3. P_is versus A_V for the programme stars.

little order (Figure 2d). The system's intrinsic polarization follows the expected pattern for an eccentric binary (Robert et al. 1989).

WR 134. This WN6 star shows the strongest line effect in our sample (Figure 1e). The polarization spectrum is variable, and the intrinsic polarization decreases from blue to red (Schulte-Ladbeck et al. 1992). The emission-line profiles vary with a 2.27-d period (McCandliss et al. 1994).

WR 135. The continuum polarization of this WC8 star is small, and there is no evidence for a line effect (Figure 1f). Although the ISP pattern is chaotic (Figure 2f), intrinsic polarization is revealed by photopolarimetric variability (Robert et al. 1989).

WR 136. Our observation, like those of S88 and SL94, does not show any line effect (Figure 1g), but Pine Bluff Observatory observations are reported to show one (Whitney et al. 1989). Robert et al. (1989) found that the star's polarization is variable, suggesting that the line effect may be easily observable only when the continuum polarization is large.

WR 137. This star is believed to be a WC7+O binary with an elliptical orbit and a period of 12.6 yr (Williams, van der Hucht & Thé 1987) . Our polarization spectrum clearly shows the line effect (Figure 1h), and the star has variable continuum polarization (Robert et al. 1989). The large binary separation ($> 100R_*$) at the time of the observation suggests that the polarization signal is intrinsic to the WR wind, rather than resulting from binary effects (Harries & Howarth 1994). Dust is formed at periastron, in a similar manner to WR 140, and wind flattening may aid dust condensation.

WR 138. A WN6 star that shows no evidence of a line effect in our data (Figure 1i), or those of S88 and SL94. However, the star is photopolarimetrically variable (Robert et al. 1989).

WR 139. V444 Cygni, the archetypal WR+O binary, shows phase-locked photopolarimetric variations (e.g., Robert et al. 1990). We observed it twice, and found the line effect to be present in one observation but undetectable in the other (Fig. 1j); the orbital phases of these observations are 0.81 and 0.05, respectively, according to the ephemeris of Kornilov & Cherepashchuk (1979; phase zero is the WR star in front). The dominant cause of the line effect evidently has its origins in binarity.

WR 140. White & Becker (1995) proposed that the WR wind of this 8 yr-period WR+O binary system is in the form of a disk (see the Introduction). Our spectropolarimetric observations (Figure 1k), and those of SL94, show no line effect. This result casts doubt on the White & Becker hypothesis.

WR 141. This WN6+O5 binary system shows the double sine-wave continuum polarization modulation expected for a close binary (Moffat, personal communication; see also Grandchamps & Moffat 1991). The star shows a small but significant line effect (see Table 2 and Figure 1l). We are not aware of any previous spectropolarimetric observations.

WR 148. A single-lined WN7 spectroscopic binary (Marchenko et al. 1996). There appears to be no detectable line effect (Figure 1m), although phase-locked polarization variability has been observed (Drissen et al. 1986).

WR 153. This short-period WR+O system shows a small PA variation with wavelength ($\pm 2°$) and has a large polarization (Figure 1n). The ISP map is moderately structured (Figure 1n), rendering interpretation difficult, but phase-locked photopolarimetric variations are indicative of intrinsic polarization (St.-Louis et al. 1988).

WR 155. This system has the shortest known period of any WR+O binary (1.6 d) and displays phase-locked photopolarimetric changes (Drissen et al. 1986). Although our survey polarization spectrum shows no line effect (Figure 1o), extensive time-series spectropolarimetry (Harries & Hilditch 1997) shows it to be present at some phases. Analysis of the time-series data indicates that the WR wind does not depart detectably from spherical symmetry.

WR 157. The line effect is not observed with certainty in this system (Figure 1p). Although there is a hint of an effect at He II $\lambda 6560$, the observed polarization is consistent with the ISP of the surrounding field stars (Figure 1p).

3 ARE THE LINE-EFFECT STARS 'SPECIAL' SYSTEMS?

We have obtained positive detections of the line effect in 4 of 16 stars in our survey. A phase-dependent line-effect may result from binarity (see for example Moffat & Piirola 1993), and this is probably the case for WR139 and WR141. The other binary systems in our sample may show the line-effect at phases other than those observed. A question of obvious interest is, are these line-effect stars 'special' systems, with a distinct wind-driving mechanism, or are all WR winds distorted, with the polarization signature of the asymmetry seen only in systems viewed at special angles? Although our sample is small, we can attempt to answer this question statistically, by studying the probability distribution of the magnitude of the line effect.

3.1 Measurements

The line effect results from dilution of a polarized continuum by unpolarized line flux, and depends on both the strength of the continuum polarization and the emission-line flux. To eliminate one variable, we will assume that the line flux is completely unpolarized (models indicate that this is a reasonable assumption for the blue wing and line core e.g. Hillier 1996); the intrinsic continuum polarization (i.e., the value that would be observed in the absence of interstellar polarization) can then be estimated from

$$P_{\rm C} \approx \Delta P(I_\ell+1)/I_\ell \quad (1)$$

where ΔP is the magnitude of the observed continuum minus line polarization vector and I_ℓ is the peak intensity of the emission line relative to the continuum.

We employed the strongest emission lines in the spectra to estimate $P_{\rm C}$ (He II λ6560Å for the WN stars and C IV λ5805Å for the WC stars). The continuum was normalized by using spline fits, and I_ℓ measured interactively. The continuum polarization at the wavelength of an emission line was estimated by a median straight-line fit to the Stokes parameters in line-free continuum bins adjacent to the line, while the emission-line polarization was measured by summing the Stokes parameters over an interactively defined bin centred on the line.

The measured polarizations and line intensities are listed in Table 2. The uncertainties are such that few $P_{\rm C}$ estimates represent firm detections, but simply to tabulate the other measurements as upper limits would be to discard useful information. (In the following analysis we used the smaller of the two polarization measurements for WR 139, as we believe this is a more accurate representation of the 'intrinsic' polarization of the WR component.)

Table 2. Polarization measurements of the survey stars. The magnitude of the continuum minus line polarization is listed (ΔP) together with the intensity of line emission line relative to the continuum (I_ℓ); the final column is a measure of the intrinsic continuum polarization ($P_{\rm C}$; see eqtn. 1). Note that the majority of measurements actually represent upper limits.

WR	ΔP	Line	I_ℓ	$\Delta P(I_\ell+1)/I_\ell$
111	0.10 ± 0.16	5805	22.8	0.10 ± 0.17
127	0.05 ± 0.18	6560	0.6	0.13 ± 0.48
128	0.03 ± 0.19	6560	1.7	0.05 ± 0.30
133	0.07 ± 0.20	6560	0.5	0.21 ± 0.60
134	0.58 ± 0.14	6560	2.1	0.86 ± 0.21
135	0.03 ± 0.21	5805	9.1	0.03 ± 0.23
136	0.02 ± 0.19	6560	3.6	0.03 ± 0.24
137	0.45 ± 0.16	5805	3.9	0.57 ± 0.20
138	0.04 ± 0.18	6560	1.2	0.07 ± 0.33
139(a)	0.03 ± 0.11	6560	0.6	0.08 ± 0.29
139(b)	0.37 ± 0.11	6560	0.7	0.90 ± 0.27
140	0.04 ± 0.18	5805	3.5	0.05 ± 0.23
141	0.25 ± 0.15	6560	1.7	0.40 ± 0.24
148	0.11 ± 0.22	6560	1.7	0.17 ± 0.35
153	0.08 ± 0.17	6560	0.6	0.21 ± 0.45
155	0.13 ± 0.17	6560	0.8	0.30 ± 0.38
157	0.18 ± 0.21	6560	2.5	0.25 ± 0.29

3.2 Methodology

To investigate the nature of the distribution of $P_{\rm C}$, we assume that the outflows are axially symmetric, and that the axes of symmetry are randomly disposed (i.e., uniformly distributed in $\cos i$); we also assume that the stellar rotation axes define the axes of symmetry, although this is largely to simplify terminology, and that

$$P_{\rm C} = P_{\rm C}(90)\sin^2 i \quad (2)$$

(Brown & McLean 1977; §5), where $P_{\rm C}(90)$ is the intrinsic continuum polarization for a system observed at $i = 90°$ (i.e., equator-on). With these assumptions, the observed distribution of $P_{\rm C}$ is determined by the probability density function of $P_{\rm C}(90)$. We therefore construct the cumulative distribution of $\Delta P(I_\ell+1)/I_\ell$, and compare this with the cumulative distribution expected for given set of assumptions regarding $P_{\rm C}(90)$.

In principle, the null hypothesis that the observed and modelled distributions are mutually consistent could be tested straightforwardly, by using the Kolmogorov-Smirnov (KS) test. In practice, this test is compromised by the presence of relatively large observational errors and, particularly, by the bias in $P_{\rm C}$; since $P_{\rm C}$ is always positive, *random* observational errors introduce a *systematic* difference between the observed and intrinsic probability distributions. We therefore conducted a Monte-Carlo (MC) analysis. For each MC cycle, we generated a simulated dataset drawn randomly from the adopted theoretical distributions of $P_{\rm C}(90)$ and i. To this we added noise based on the observed uncertainties, and constructed the cumulative probability distribution for these noisy, model data. By requiring $P_{\rm C}$ always to be positive, we automatically take into account the bias in that quantity.

For each MC cycle we evaluated the KS statistic, i.e., the modulus of the maximum difference in $N/N_{\rm Tot}$ between the cumulative distributions of the simulated dataset and a reference distribution. Comparison of the KS statistic similarly calculated for the observed distribution with the distribution of KS statistic from the simulations allows us to estimate the confidence with which the null hypothesis can be rejected.

In order to improve the statistical efficiency of the test, we used the average of the MC model distributions as the reference distribution. This is necessary because the biased nature of $P_{\rm C}$ means that the average of the model distributions is *not* identical to the assumed intrinsic distribution. The deviations of these two distributions depend on the magnitude of the errors relative to the 'size' of $P_{\rm C}(90)$ (as parameterized by some suitable summary statistic of central tendency, for example). In consequence of this, the size of $P_{\rm C}$ must be treated as a free parameter, even though the comparison of cumulative probabilities is based on distributions which are normalized to their maximum values. We optimized that free parameter by requiring that the median maximum polarization in the MC-replicated model samples be equal to the maximum observed value of P_C. This optimization (and, more generally, the output of the MC simulations) depends on the probability distribution adopted for the observational errors; we carried out all calculations twice, assuming uniform and Gaussian distributions. The qualititative conclusions summarized in the following subsection hold true in each case, although, as expected, the numerical results differ in detail.

3.3 Results

The simplest possible null hypothesis is that all stars have the same intrinsic continuum polarization when observed equator-on, i.e.,

$$P_C(90) = \text{constant}. \tag{3}$$

The (intrinsic) cumulative distribution for this parent population is described by a simple analytical function:

$$N\left(P_C \leq P(x)\right)/N_{\rm Tot} = 1 - \left(1 - P(x)\right)^{1/2}, \tag{4}$$

where $P(x) = P_C/P_C(90)$. The best estimate of $P_C(90)$, optimized in the sense described above, is 0.64% (for observational errors uniformly distributed).

We find that the null hypothesis of constant $P_C(90)$ can be rejected with $> 99.9\%$ confidence (a conclusion which remains true if the binary line-effect systems are eliminated from the sample). As is evident from Fig. 4, this is because of an excess of low-polarization systems in the observations; we conclude that our dataset is not consistent with a fixed level of intrinsic polarization modified by random orientations of the axes of symmetry.

After a constant value, the next simplest distribution we can adopt for $P_C(90)$ is a uniform probability density between zero and some value $P_C(\max)$. This gives an observed distribution which is biased towards smaller observed polarizations than the constant-$P_C(90)$ model (since large P_C requires large $P_C(90)$ *and* large i, while small P_C can result from small $P_C(90)$ *or* small i). The cumulative distribution function based on this null hypothesis is also shown Figure 4, optimized for $P_C(\max) = 0.91\%$. As expected, the agreement with observations is better, but is still not particularly convincing; the observed and model distributions differ with 92% confidence if the full dataset is considered, increasing to 98% if WRs 139 and 141 are excluded from the sample.

More elaborate model distributions are increasingly ad hoc, but the excess of observed low-polarization systems, and the possibility of physical mechanism involving a threshold 'switch', motivate us to explore one further class of model. For these calculations we assume that $P_C(90)$ is zero for some fraction f of the parent population, and is uniformly distributed for the remainder, thus giving a family of cumulative distributions characterized by only one additional parameter. We find that this family is formally consistent with the observations over the large range $0 \leq f \leq 0.97$ – not a surprising result, given that the uniform-distribution model ($f \equiv 0$) is already only marginally ruled out. However, the most satisfactory results are achieved for moderately large fractional populations of zero-polarized stars; the best-fit (minimum-KS) solution is obtained with $f = 0.85$ (and $P_C(\max) = 1.75\%$ for uniformly distributed observational errors). The mean MC distribution for this model is illustrated in Fig. 4.

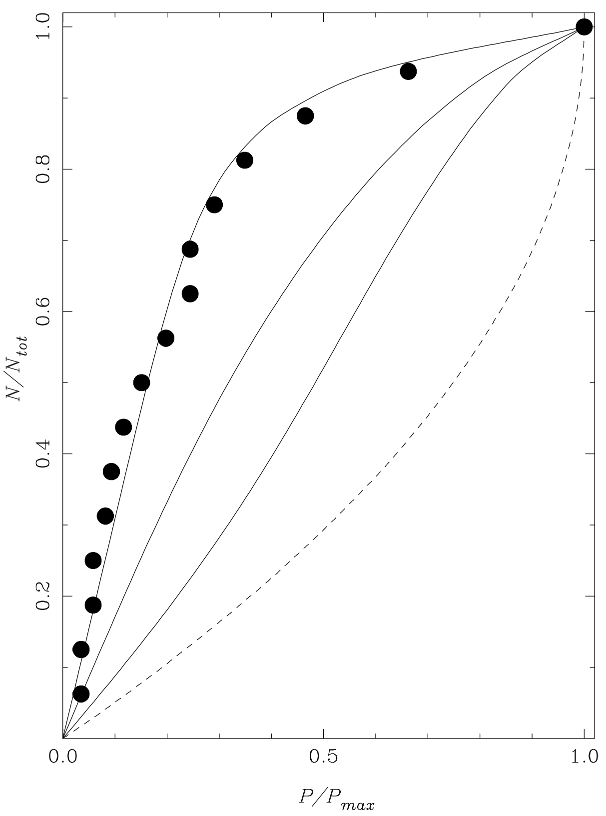

Figure 4. The cumulative distribution of observed continuum polarization, P_C (filled circles). The cumulative distribution for a parent population of stars with constant polarization observed at random viewing angles is shown as the dashed line, while the lowest continuous line shows the same distribution corrected for observational bias (as described in § 3.2). Similarly corrected cumulative distributions are shown for a parent population having intrinsic polarizations uniformly distributed from zero (centre continuous line) and for a parent population wherein 85% of stars have zero polarization and the remainder have polarizations uniformly distributed from zero (top line).

.

We conclude that the WR stars most probably have a distribution of intrinsic polarizations which is biased towards small values. About 20% of the enlarged sample summarized in § 4 show the line effect, but there may be concealed selection effects in that sample; our best estimate is, therefore, that ∼15–20% of WRs have 'significant' intrinsic polarizations (that is, larger than our median error of 0.3% in P_C), with the largest values in the parent population expected to be less than about 1.5–2%. Such a distribution would be consistent with a model where global wind asymmetries arise only in the fastest rotators, while the upper limit to intrinsic polarization allows us us to put limits on the maximum degree of asymmetry.

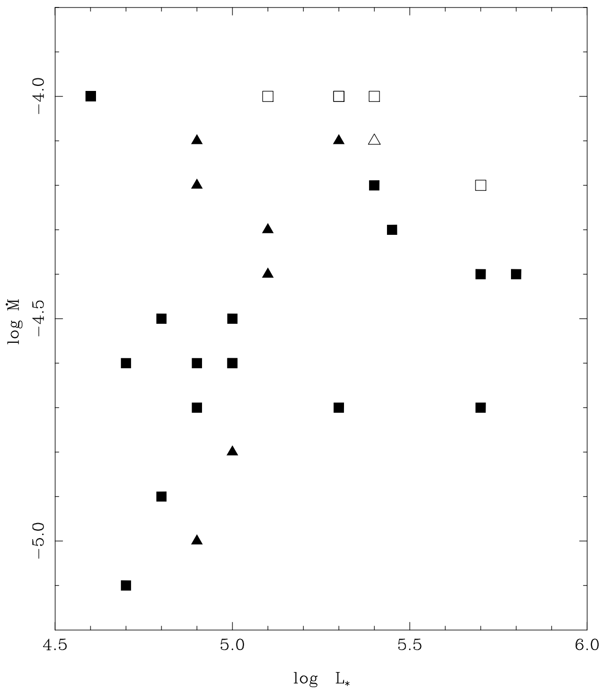

Figure 5. The two samples plotted in the luminosity–mass-loss rate plane. Stars with spherical and non-spherical winds are plotted with filled and open symbols respectively. WN stars are plotted as squares while WC stars are plotted as triangles.

4 PHYSICAL CHARACTERISTICS OF LINE-EFFECT STARS

In the standard model used in the spectroscopic analysis of WR stars, the temperature parameter is, essentially, based on the ratio of He I to He II line strengths, while the line strengths relative to the continuum give a density-related parameter which depends on the mass-loss rate, terminal velocity, and stellar radius. Since the line strengths are, to first order, dependent on density squared (the dominant populating mechanisms being recombination and, less frequently, collisional excitation), and since any departure from spherical symmetry (on small or large scales) will increase the 'clumping factor', $\langle n^2 \rangle / \langle n \rangle^2$, it is of interest to ask whether stars showing evidence for wind asymmetries also show discrepant physical parameters, including mass-loss rates.

To address this question, we combined the results of our survey with literature data (Table 3). We divided this enlarged sample into two groups: stars that do not show the line effect, and single WR stars that do. We included WRs 139, 141, and 155 in the former category, since for these stars the line effect appears to have its origins in binary interaction, and put WR 137 in the latter category, since the wide binary separation suggests that the polarimetric signal is intrinsic to the Wolf-Rayet. [Note that the binary systems in the 'no line effect' category may still show a phase-dependent line-effect.] We rejected stars for which standard-model analyses are not available in the literature, giving final subsample sizes of 23 and 6 stars, respectively.

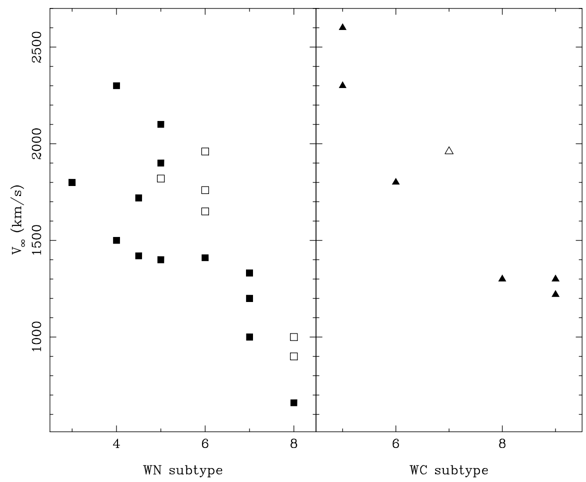

Figure 6. The terminal velocities of the WR winds plotted as a function of spectral subtype. The symbols are as for Figure 5.

Physical parameters for the enlarged sample are listed in Table 3.

When the data are plotted in the luminosity–mass-loss rate plane (Fig. 5) the line-effect stars are clustered in a small region at $\log L = 5.4$ and $\log \dot{M} = -4.1$, at the top of the mass-loss range. This suggests that, as expected, the increase in clumping factor associated with the asymmetry in these stars' winds leads to an overestimate of $\dot{M}$. However, the mass-loss rates (and luminosities) derived from standard-model analyses are quite model dependent. Radio-continuum emission gives mass-loss rates more straightforwardly, and offers a useful, largely independent, estimate of $\dot{M}$. Howarth & Schmutz (1992) have shown that standard-model and radio analyses give mass-loss rates in good mutual accord (when common distances and terminal velocities are adopted).

We found radio observations in the literature for all 6 line-effect systems, and for 11 systems with no line effect (4 of these having radio upper limits). We computed mass-loss rates from these data using the formalism given by Wright & Barlow (1975), adopting terminal velocities, distances, and chemistries from optical analyses (cf. Table 3). We followed the treatment given by Howarth & Schmutz (1992) in respect of ionization in the radio-emitting region. The results are summarized in Table 4. The average difference in (optical−radio) logarithmic mass-loss rates for the stars with no line effect is $+0.11 \pm 0.23$ (s.d.), while the line-effect stars give $+0.12 \pm 0.21$; the grand average is $+0.10 \pm 0.22$. We therefore confirm that the line-effect stars have apparently high mass-loss rates (Fig. 5), and also the result of Howarth & Schmutz (1992) that mass-loss rates derived from radio and optical analyses are in good agreement.

The optical line emission and radio continuum emission are both proportional to density squared; thus the general agreement between standard-model and radio mass-loss rates does not imply that both are correct, but simply that the clumping factors are similar at the radii of optical depth $\sim$1 – that is, around $\sim 10^1 R_*$ for the optical, and $\sim 10^3 R_*$

Table 3. Physical parameters for WR stars with published spectropolarimetry. Spectral types are from Smith, Shara & Moffat (1990) and Smith, Shara & Moffat (1996). The temperatures (T_*) and radii (R_*) refer to the central core (where the Rosseland optical depth > 10). Parenthesised values for M_v indicate field stars. 'Ref. 1' is the source of physical parameters, and 'Ref. 2' the source of the spectropolarimetric data. The references are: HKW, Hamann, Koesterke & Wesselowski (1995); HS92, Howarth & Schmutz (1992); H97, Harries et al. (1997); KH95, Koesterke & Hamann (1995); nWR, this study; SL94, Schulte-Ladbeck (1994); S88, Schmidt (1988); and W89, Whitney et al. (1989).

WR	Spec. type	T_* (kK)	M_v	R_* ($R_\odot$)	$\log L_*$ ($L_\odot$)	v_∞ (km s^{-1})	$\log \dot{M}$ ($M_\odot$ yr^{-1})	Ref. 1	Ref. 2
Single stars showing a line effect									
6	WN4b	70	−4.6	2.5	5.1	1820	−4.0	H97, HS92	SL94
16	WN8h	31	(−6.7)	25	5.7	900	−4.2	HKW	SL94
40	WN8h	31	(−5.7)	16	5.3	1000	−4.0	HKW	SL94
134	WN6b	65	−4.8	3.6	5.3	1960	−4.0	HS92	SL94
136†	WN6	55	−5.0	5.3	5.4	1760	−4.0	HS92	W89
137	WC7+OB	40	−5.4	11	5.4	1960	−4.1	HS92	nWR
Stars showing no line effect									
14	WC7	86	−3.8	1.3	4.9	1800	−4.2	KH95	SL94
18	WN4b	90	−3.3	1.3	5.0	2100	−4.5	HS92	SL94
24	WN6ha	32	−6.3	23	5.7	1200	−4.7	HS92	SL94
78	WN7h	32	−6.5	26	5.7	1200	−4.4	HS92	SL94
104	WC9	30	−4.5	10	4.9	1220	−5.0	HS92	S88
110	WN5-6b	65	−3.5	1.6	4.6	3190	−4.0	HS92	SL94
111	WC5	62	−3.7	2.7	5.0	2000	−4.3	KH95	SL94, nWR
121	WC9	30	−5.2	13	5.1	1300	−4.4	HS92	S88
127	WN3b+O9.5V	45	−3.3	3.7	4.7	2300	−4.6	HS92	S88, nWR
128	WN4(h)	36	(−3.6)	5.7	4.7	1500	−5.1	HKW	nWR
133	WN5o+O9I	35	−4.5	8.6	5.0	1420	−4.6	HS92	S88, nWR
135	WC8	76	−4.2	2.6	5.3	1300	−4.1	KH95	nWR
138	WN5o+B?	32	−5.4	15	5.3	1400	−4.7	HS92	S88, nWR
139*	WN5o+O6	34	−4.2	8.3	4.9	1900	−4.7	HS92	nWR
141*	WN6+O5	40	−5.4	11	5.4	1650	−4.2	HS92	nWR
143	WC4	51		4.3	5.0	3200	−4.8	KH95	S88
148	WN8h	31	(−6.7)	27	5.8	1000	−4.4	HKW	nWR
150	WC5	71	−3.7	1.9	4.9	2600	−4.1	KH95	S88
152	WN3(h)	40	−3.6	5.5	4.8	1800	−4.9	HS92	S88
153	WN6o/CE+O6I	35	−4.3	6.9	4.8	1410	−4.5	HS92	SL94, nWR
155*	WN6o+O9II/Ib	34	−4.5	9.0	5.0	1330	−4.6	HS92	nWR
156	WN8h	30	(−6.7)	27	5.7	700	−4.3	HKW	S88
157	WN5o (+B1 II)	35	−4.3	7.7	4.9	1720	−4.6	HS92	nWR

† WR 136 does not show the line effect in our data, nor in those of S88 and SL94.
* WRs 139, 141 and 155 display line effects due to binarity.

for the radio. Since we have no reason to suppose that the line-effect stars differ from the majority in their small-scale structure, we can take this as evidence that the large-scale structure is preserved over this range in radii.

Simple models suggest that axially symmetric winds should have latitude-dependent outflow velocities. Since terminal velocities measured from homogeneous datasets show a good correlation with spectral subtype for both WN and WC sequences (e.g., Howarth & Schmutz 1992), it is of interest to investigate if the line-effect stars are exceptional in this regard. Terminal velocities of the WN and WC stars are plotted against subtype in Figure 6. There is no obvious difference between the measured terminal velocities of the stars with demonstrably non-spherical winds and the remainder, although the samples are small (particularly for the WC sequence). The line-effect stars are also unexceptional when surface mass flux is plotted against temperature parameter, T_* (Fig.7; cf. Howarth & Schmutz 1992).

5 RADIATIVE-TRANSFER MODELS

In order to relate the observed $P_{\rm C}$ values to physical characteristics of the stellar winds we have used the Monte-Carlo code described by Hillier (1991) to compute polarization spectra. We used a source function computed for the He II λ5412 emission line by Crowther (personal communication) using Hillier's Standard Model code (Hillier 1990), as an input for the analysis, and adopted a simple function for the latitude dependence of wind density:

$$\rho(\mu) = k(1 - x|\mu|^p), \tag{5}$$

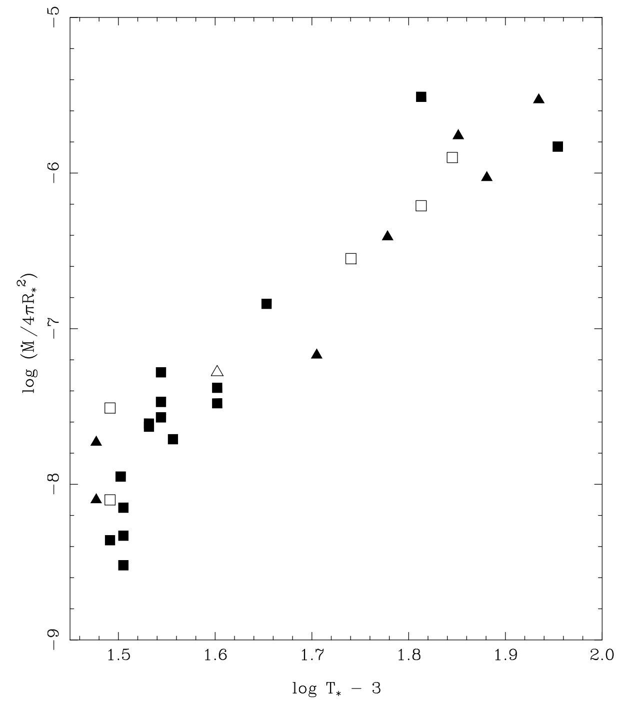

Figure 7. The logarithm of surface mass flux (in $\mathrm{M_\odot\,yr^{-1}R_\odot^{-2}}$) as a function of $\log T_*$. The symbols are as for Figure 5.

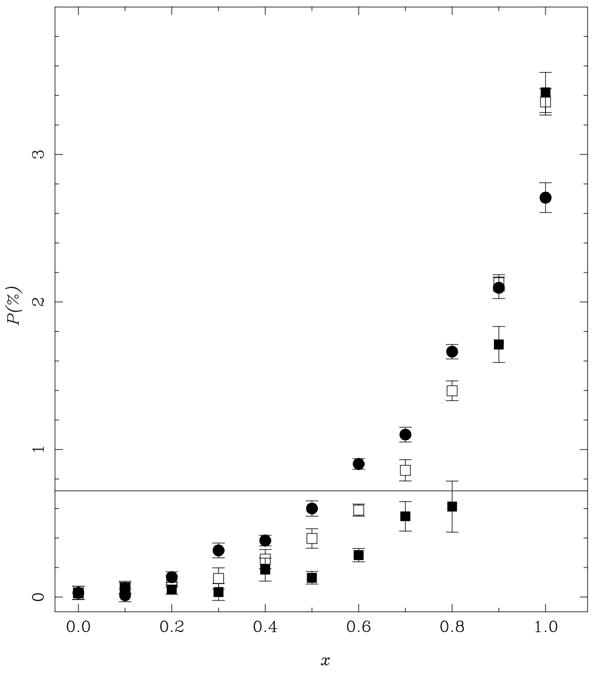

Figure 8. Continuum polarization of the models as a function of x for $p = 0.5$ (filled squares), $p = 1$ (open squares) and $p = 2$ (filled circles). The solid line represents the mean polarization of the 'single' line-effect stars (0.72%). Error bars on the measurements are 1σ.

Table 4. Radio mass-loss rates for the enlarged WR sample, calculated using the terminal velocities and distances listed in Table 3. References are: LCK (Leitherer, Chapman & Koribalski 1995), ABCT (Abbott, Bieging, Churchwell & Torres 1986), BAC (Bieging, Abbott & Churchwell 1982), H92 (Hogg 1982), and DHI (Dickel, Habing & Isaacman (1980).

WR	S_ν (mJy)	ν (GHz)	Ref.	$\log \dot{M}$ ($M_\odot \mathrm{yr}^{-1}$)
		Line-effect stars		
6	1.0	4.9	H82	−4.21
16	1.8	8.6	LCK	−3.94
40	2.5	8.6	LCK	−4.08
134	0.8	4.9	H82	−4.18
136	1.6	4.9	DHI	−4.11
137	0.4	4.9	BAC	−4.50
		Other stars		
24	1.1	8.6	LCK	−4.46
78	1.4	4.9	ABCT	−4.44
110	1.0	4.9	BAC	−4.08
111	0.3	4.9	BAC	−4.77
121	< 0.3	4.9	BAC	< −4.34
133	< 0.3	4.9	H82	< −4.63
135	0.6	4.9	H82	−4.44
138	0.6	4.9	BAC	−4.70
139	0.3	4.9	BAC	−4.65
141	0.6	4.9	ABCT	−4.43
143	< 0.4	4.9	ABCT	< −4.90

where $\mu = \cos\theta$ and θ is the colatitude. The normalization parameter k was chosen to preserve the same mass-loss rate as a spherical model. The line and continuum opacities were varied as ρ^2, and the electron-scattering opacity linearly with ρ. Polarization spectra were computed for $i = 90°$ and $p = 0.5$, 1, and 2, with $x = 0.0$–1.0 at steps of 0.2. We also calculated models as a function of inclination for $p = 1, x = 1$. The models were computed using 5×10^6 photon packets, employing variance-reduction techniques to obtain improved statistics (cf. Hillier 1991).

Figure 8 illustrates the variation of continuum polarization with p and x. The solid horizontal line indicates the observed continuum polarization of the two 'single' line-effect stars in our sample (WRs 134 and 137). By comparing these calculations with the results of § 3, we can deduce that (*i*) ∼80% of stars have winds with equator-to-pole density ratios less than about 1.5; (*ii*) the observed line-effect stars are consistent with equator-to-pole density ratios of 2–3; and (*iii*) stars with equator-to-pole density ratios in excess of ∼5 are rare, if they occur at all.

These conclusions rely on the validity of the models. We used WR 134, which has the largest line effect in our sample, to provide a specific point of comparison of these models with observations. We used the $x = 0.6, p = 2, i = 90°$ model, which has a continuum polarization of 0.90% (cp. 0.86% for the observations).

The primary difficulty in making a comparison is accounting for the interstellar polarization. We have already

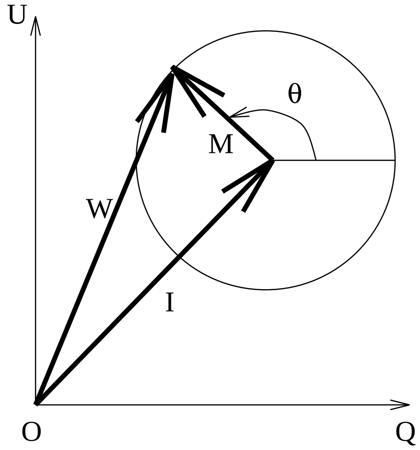

Figure 9. The observed continuum polarization (W) is the vector sum of the interstellar polarization (I) and the model continuum polarization (M) at an arbitrary position angle (θ).

shown (see §2.1) that the ISP patterns of the field stars about most of the surveyed WR systems (including WR134) display little or no coherence. We must therefore adopt a different approach for estimating the ISP. We assume that the magnitude of the model continuum polarization is an accurate representation of the magnitude of the intrinsic polarization of WR134. The observed vector is then the vector sum of the ISP and model continuum polarization at an arbitrary position angle, θ (this is shown schematically in Figure 9). We may then fit the model to the observations, with one free parameter (θ), using traditional numerical techniques (in this case a golden section search for a χ^2 minimum).

We performed the above minimization on the observation of WR134, defining continuum bins either side of the line profile. The resulting ISP was $\overline{q} = 0.34\%$ and $\overline{u} = -0.09\%$, with $\theta = 4°$ and a reduced χ^2 of 2.1.

The intensity spectra are in good overall agreement (Fig. 10), although the line strength is slightly too strong in the model. The largest difference, however, is the strength of the electron-scattered redwards line wing, which is not apparent in the observations but which the model predicts should be visible over ∼100Å.

The depolarization in the emission line is generally well modelled, but it is clear that polarization in the far-red electron-scattered wing is too strong in the model. We applied the ISP fitting technique to the whole $[p, x]$ grid and found similar results, with no model yielding a satisfactory fit to both the core depolarization and the strong model wing. Further models were computed for the He II λ6560 line, and although contamination by the λ6683 helium line made comparison between model and observation difficult it was clear that the model red-wing was more strongly polarized than observation. [We note that the depolarization in the λ6560 line is well modelled, providing post priori justification for its choice as a continuum polarization diagnostic in Section 3.1.]

The discrepancy between the *intensity* of the red-wings of the models and observations may be considered as subjective, since the comparison rests upon the rectification of a

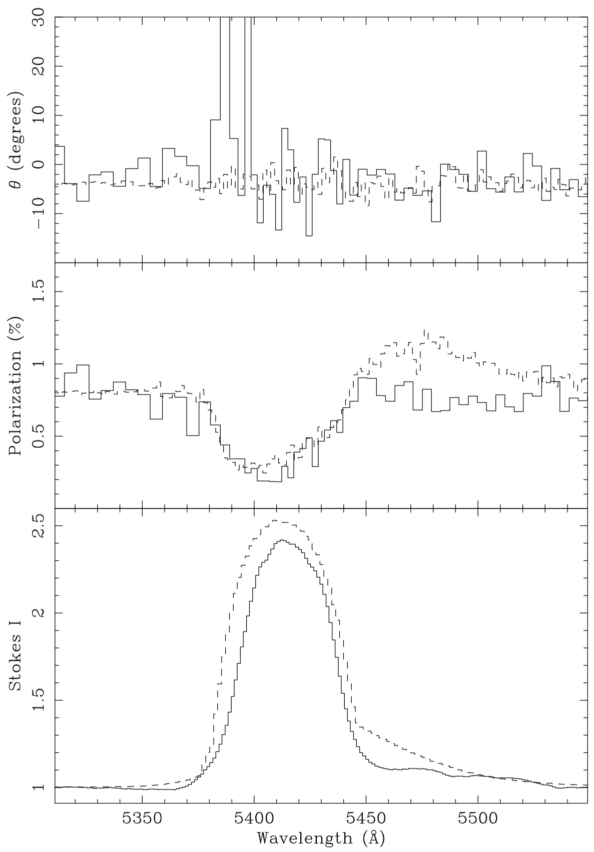

Figure 10. A comparison between the observed (solid line) and model $p = 2, x = 0.6$ (dashed line) polarization spectra of the λ5412 emission line of WR134. The observed polarization spectrum has been correct for ISP (see text), and is binned to a constant error of 0.1% in P.

significantly curving continuum (see Figure 1e), although we were unable to reproduce the strong red-wing with within reasonable continuum normalization parameters. The difference in polarization magnitude is a more secure result, since it is independent of the continuum normalization.

In order to reconcile the observations and the models the mass-loss rate must be decreased (to reduce the electron scattering column) while the clumping factor must be increased (to conserve the line emission). If clumping is invoked, however, a greater asymmetry is required to produce the same continuum polarization (since the electron-scattering opacity is less, and in the optically thin limit $P \propto \tau_{es}$). Hence our current model may underestimate the asymmetry in the wind of WR134.

Finally, we can use the models to check the assumption that $P \propto \sin^2 i$ (§ 3.2); Brown & McLean (1977) obtained this result in the optically thin limit for the contin-

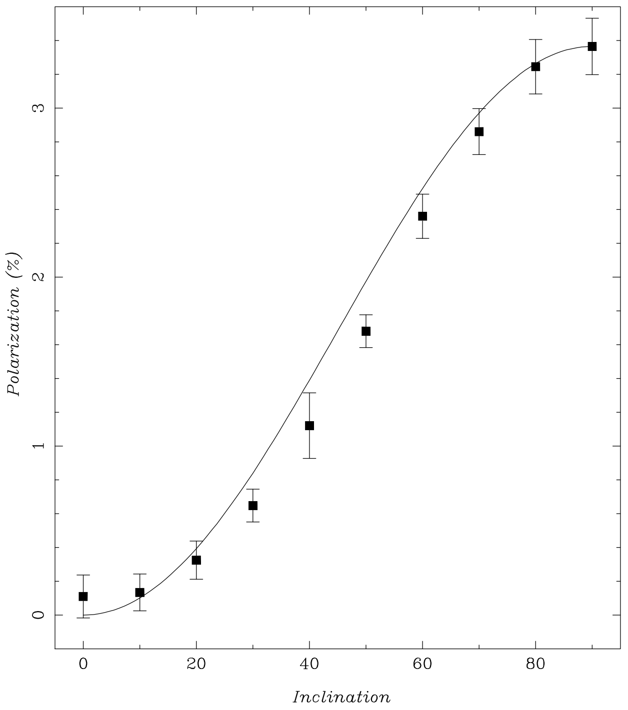

Figure 11. The inclination dependence of the $x = 1$, $p = 1$ model. The continuum polarization values are plotted as filled squares with 1-σ error bars. The solid line represents the $P_{\rm C}(90)\sin^2 i$ curve predicted by the Brown & McLean (1978) analysis.

uum polarization of an axisymmetric envelope⋆. In Figure 11 we plot continuum polarization against inclination for the $p = 1, x = 1$ model. A $P_{\rm C}(90)\sin^2 i$ curve gives a satisfactory fit to the data, with only minor discrepancies which are attributable to occultation and multiple-scattering effects (the wind is optically thick in the continuum at $\sim \lambda5412$, and the mean number of continuum scatterings is 1.7 per photon packet).

6 DISCUSSION

Our observations indicate a significant minority of WR systems have winds which have structure on large scales. These systems appear to occupy a small range in luminosity and mass-loss rate, although mass-loss rates derived for line-effect systems are subject to correction for latitude-dependent density structure. The line-effect stars do not appear to have discrepant terminal velocities (which are model-independent quantities) or surface mass fluxes (which are model dependent).

Although other geometries (e.g., polar plumes, azimuthal wind structures) are consistent with the data, our working hypothesis is that the line effect is due to equatorial density enhancements, as predicted from simple kinematic considerations (Bjorkman & Cassinelli 1993)†. Ignace, Cassinelli & Bjorkman (1996) find that WR stars do not show significant wind-compression effects below a distinct rotational velocity (expressed as a fraction of the critical velocity); above that limit, equatorially-compressed winds form. They propose that the line-effect stars are whose rotational velocity exceeds the critical limit, i.e., that they represent the high-velocity tail of the rotational-velocity distribution.

Observational evidence for rapid rotation of WR stars is sparse, primarily because the stellar winds are normally optically thick in the continuum, shrouding the hydrostatic layers. Nonetheless, projected rotational velocities of 500 km s^{-1} and 150–200 km s^{-1} have been reported for WRs 138 and WR 3 (Massey 1980; Massey & Conti 1981), although the association of the measured features with the WR core has been questioned as both systems may be long-period binaries (Annuk 1991; Smith, Shara & Moffat 1996).

Although there is only limited evidence for rapid rotation in WR stars, their precursors – the O stars – are well known to show rotational velocities of up to several hundred km s^{-1}(Conti & Ebbets 1977; Howarth et al. 1997). Moreover, there is direct evidence, both from spectropolarimetry (ζ Puppis; Harries & Howarth 1996b) and from line-profile morphology (HD 93521, Howarth & Reid 1993; HD 191423, Howarth et al. 1997), that this rotation modifies the geometry of O-star winds. Angular momentum may be lost on evolutionary time-scales, by magnetic braking or mass-loss, but it is clearly plausible that WR cores should retain significant rotational velocity, and that this should be associated with nonspherical wind geometries.

Indirect evidence for rapid rotation may be derived from time-series observations; rotational modulation has been identified in the OB stars ζ Puppis (Moffat & Michaud 1981; Howarth, Prinja & Massa 1995), θ Ori C (Stahl et al. 1996), and HD 64760 (Prinja, Massa & Fullerton 1995), and similar signals in observations of Wolf-Rayets can be used to estimate rotation periods. Periodic variability has been documented for five of the seven line-effect stars in Table 3:

WR 6 (EZ CMa) shows 3.77-d periodic variability in photometry, photopolarimetry, and spectroscopy (e.g., Lamontagne, Moffat & Lamarre 1986; McLean 1980; St.-Louis et al. 1996), although the shape of the photometric and polarimetric light-curves is unstable over time-scales of weeks.

WR 16 has a litany of variability studies: Moffat & Niemela (1982) found a period of 10.73 d from intermediate-band photometry, subsequently confirmed by Lamontagne & Moffat (1987), although the primary comparison star used in both studies is variable (Manfroid, Gosset & Vreux 1987). Balona, Egan & Marang (1989) identified a period of 17.54d using a different comparison object.

WR 40, the second WN8 line-effect star in our sample, was classified WR+c by Moffat & Isserstedt (1980), who found a period near 4.8 d and a 10-km s^{-1}radial-velocity

⋆ This relationship assumes a point-source illumination, and thus neglects the occultation of scattering material by a finite disk; Fox (1991) has demonstrated that occultation effects are only significant in highly-flattened geometries.

† The most recent models actually predict equatorial *rarefaction* (Owocki, Cranmer & Gayley 1996); however, observations of the most rapidly rotating O-type stars are not consistent with such models (e.g., Howarth & Reid 1993).

Table 5. Rotational velocities for the line-effect stars. Radii are from Table 3, while the periods are given in §6. The ratios of rotational to critical velocity are given for M_*=10M$_\odot$ (where $v_{\rm crit} = (GM/R)^{\frac{1}{2}}$).

WR	Period (d)	R_* (R$_\odot$)	$v_{\rm e}$ (km s^{-1})	$v_{\rm e}/v_{\rm crit}$ (%)
6	3.77	2.5	34	7
16	17.5	25	72	26
40	12.3/17.5	16	65/46	19/13
134	2.27	3.6	80	11
136	4.5	5.3	60	10

semi-amplitude. Matthews & Moffat (1994) analysed several photometric datasets for this object and identified two periods (12.3 d and 17.5 d), which they argued are associated with the binary period and asynchronous rotational modulation (although which period is associated with binarity and which with rotation is unclear), while a frequency analysis of the polarimetry reported by Drissen et al. (1987) yielded a period of 18.9 d.

WR 134 shows emission-line variability with a 2.27-d period according to McCandliss et al. (1994).

WR 136 has a period of ~ 4.5d according to Koenigsberger et al. (1980), although this estimate is based on a small sample of spectra. Spectroscopy yields a period of 0.45 d or 0.31 d, however, with a semi-amplitude of 32 km s^{-1}(Vreux, Andrillat & Gosset 1985); the short periods could be associated either with non-radial pulsation or with orbital motion.

We found no short time-scale photometric or spectroscopic studies of WR 137 in the published literature.

If we make the plausible assumption that the spectroscopic and photometric variability of the line-effect stars arises from rotational modulation, then we can estimate their rotational velocities. The principal difficulty is in defining the stellar radius. We could assume that the variability is seated in the hydrostatic core, and take the radius R_* (normally defined by assuming projecting a β-law velocity structure back into the star and locating the radius at which the Rosseland optical depth is greater than 10–20). An alternative would be to take the radius as the thermalization radius of the particular continuum sampled (photometry) or of the greatest line emission (spectroscopy). For simplicity, we adopt the former approach, with the caveat that the radii are computed from spherical-wind models (Table 3). The inferred rotational velocities are listed in Table 5.

The ratios of rotational to critical velocity are also listed in Table 5; although the values of $v_{\rm crit}$ are uncertain (depending on an assumed mass), it is of note that all the ratios are close to the 11% value which Ignace, Cassinelli & Bjorkman (1996, hereinafter ICB96) estimate as lower limit for wind-compression effects in WR stars. We note, however, that the ICB96 models assume a rather large value of β (=3) for the WR velocity law. This has the effect of keeping the material close to the sonic point for longer, allowing the effects of rotation to bring the material down to the equator to form a compressed zone. Such a slowly accelerating wind may be physically unrealistic, since it requires a delicate balance between gravitational and radiative forces–a lower value of β would mean that higher rotation rates are required before a significant density contrast is produced at the equator.

We conclude that it is plausible that the line-effect stars represent WRs with the most rapid rotation. Searches for rotationally-modulated variability in the line-effect star WR 137 would be useful to test this hypothesis, while spectropolarimetric observations of additional stars should yield further line-effect systems and allow stronger conclusions to be drawn concerning the incidence of wind distortion in Wolf-Rayets.

ACKNOWLEDGMENTS

We thank Paul Crowther for providing an emission-line source function. The William Herschel Telescope is operated on the island of La Palma by the Royal Greenwich Observatory at the Spanish Observatorio del Roque de los Muchachos of the Instituto de Astrofisica de Canarias. The computational work was performed at the St. Andrews and UCL nodes of the UK Starlink network. TJH was funded by PPARC postgraduate and postdoctoral research grants.

REFERENCES

Abbott, D.C., Bieging, J.H., Churchwell, E., Torres, A.V., 1986, ApJ, 303, 239

Allen, C.W., 1973, Astrophysical Quantities (3rd edition), Athlone Press

Annuk, K., 1991, in 'Wolf-Rayet Stars and Interrelations with Other Massive Stars in Galaxies', IAU Symp. 143, K.A. van der Hucht & B. Hidayat (eds), Kluwer (Dordrecht), p. 245

Balona, L.A., Egan, J., Marang, F., 1989, MNRAS, 240, 103

Bieging, J.H., Abbott, D.C., Churchwell, E.B., 1982, ApJ, 263, 207

Bjorkman, J.E., Cassinelli, J.P., 1993, ApJ, 409, 429

Brown, J.C., McLean, I.S., 1977, A&A, 57, 141

Cassinelli, J.P., 1992, in 'Nonistropic and Variable Outflows from Stars', L. Drissen, C. Leitherer & A. Nota (eds), ASP Conf. Series 22, p. 134

Conti, P.S., Ebbets, D., 1977, ApJ, 213 438

Crawford, D.L. 1975, AJ, 80, 955

Crawford, D.L. 1978, AJ, 83, 48

Crawford, D.L. 1979, AJ, 88, 1858

Dickel, H.R., Habing, H.J., Isaacman, R., 1980, ApJ, 283, L39

Drissen, L., Lamontagne, R., Moffat, A.F.J., Bastien, P., Seguin, M., 1986, ApJ, 304, 188

Drissen, L., St.-Louis, N., Moffat, A.F.J., Bastien, P., 1987, ApJ, 322, 888

Fox, G.K., 1991, ApJ, 379, 663

Grandchamps, A., Moffat, A.F.J., 1991, in 'Wolf-Rayet Stars and Interrelations with Other Massive Stars in Galaxies', IAU Symp. 143, K.A. van der Hucht & B. Hidayat (eds), Kluwer (Dordrecht), p. 258

Hamann, W.-R., Koesterke, L., Wesselowski, U., 1995, A&A, 299, 151

Harries, T.J., Howarth, I.D., 1994, in 'Instability and Variability of Hot-Star Winds', A.F.J. Moffat, S.P. Owocki, A.W. Fullerton, N. St-Louis (eds), Kluwer (Dordrecht), p. 365

Harries, T.J., Howarth, I.D., 1996a, A&AS, 119, 61

Harries, T.J., Howarth, I.D., 1996b, A&A, 310, 533

Harries, T.J., Hilditch, R.W., 1997, MNRAS, 291, 544

Harries, T.J., Howarth, I.D., Schulte-Ladbeck, R., Hillier, D.J., 1997, MNRAS, (in preparation)
Hauck, B., Mermilliod, J.C., 1990, A&AS, 86, 107
Heintze, J.R.W. 1973, in IAU Symp. 54 (Reidel), 231
Hillier, D.J., 1991, A&A, 247, 455
Hillier, D.J., 1994, in 'Wolf-Rayet Stars: Binaries, colliding winds, evolution', IAU Symp. No. 163, K.A. van der Hucht & P.M. Williams (eds), Kluwer (Dordrecht), p. 116
Hillier, D.J., 1990, A&A, 231, 116
Hillier, D.J., 1996, A&A, 308, 521
Hogg, D.E., 1982, in IAU Symp. 99: Wolf-Rayet Stars: Observations, Physics and Evolution, C.W.H. de Loore, A.J. Willis (eds), Reidel (Dordrecht), p. 221
Howarth, I.D., Schmutz, W., 1992, A&A, 261, 503
Howarth, I.D., Reid, A.H.N., 1993, A&A, 279, 148
Howarth, I.D., Prinja, R.K., Massa, D., 1995, ApJ, 452, L53
Howarth, I.D., Siebert, K.W., Huassin, G.A., Prinja, R.K., 1997, MNRAS, 284, 265
Ignace, R., Cassinelli, J.P., Bjorkman, J.E., 1996, ApJ, 459, 671
Klare, G., Neckel, T., 1977, A&AS, 27, 215
Koenigsberger, G., Firmani, C., Bisiacchi, G.F., 1979, Rev. Mex. Astron. Astrof., 5, 45
Koesterke, L., Hamann, W.-R., 1995, A&A, 299, 503
Kornilov, V.G., Cherepashchuk, A.M., 1979, Sov. Astr. Letters., 5, 214
Lamontagne, R., Moffat, A.F.J., Lamarre, A., 1986, AJ, 91, 925
Lamontagne, R., Moffat, A.F.J., 1987, AJ, 94, 1008
Leitherer, C., Chapman, J.M., Koribalski, B., 1995, ApJ, 450, 289
Manfroid, J., Gosset, E., Vreux, J.M., 1987, A&A, 185, L7
Marchenko, S.V., 1994, in 'Instability and Variability of Hot-Star Winds', A.F.J. Moffat, S.P. Owocki, A.W. Fullerton, N. St-Louis (eds), Kluwer (Dordrecht), p. 169
Marchenko, S.V., Moffat, A.F.J., Lamontagne, R., Tovmassian, G.H., 1996, ApJ, 461, 386
Massey, P., 1980, ApJ, 236, 526
Massey, P., Conti, P.S., 1981, ApJ, 244, 173
Matthews, J.M., Moffat, A.F.J., 1994, A&A, 283, 493
Mathewson, D.S., Ford, V.I., Klare, G., Neckel, T., Krautter, J. 1978, Bulletin CDS, 14, 115
McCandliss, S.R., Bohannan, B., Robert, C., Moffat, A.F.J., 1994, in 'Instability and Variability of Hot-Star Winds', A.F.J. Moffat, S.P. Owocki, A.W. Fullerton, N. St-Louis (eds), Kluwer (Dordrecht), p. 155
McLean, I.S., 1980, ApJ, 236, L149
McLean, I.S., Coyne, G.V., Frecker, J.E., Serkowski, K., 1979, ApJ, 231, L141
Mermilliod, J.C. 1987, A&AS, 71, 413
Moffat, A.F.J., Isserstedt, J., 1980, A&A, 91, 147
Moffat, A.F.J., Michaud, G., 1981, ApJ, 251, 133
Moffat, A.F.J., Niemela, V.S., 1982, A&A, 108, 326
Moffat, A.F.J., Piirola, V., 1993, ApJ, 413, 724
Moffat, A.F.J., Drissen, L., Lamontagne, R., Robert, C., 1988, ApJ, 334, 1038
Owocki, S.P., Cranmer, S.R., Gayley, K.G., 1996, ApJ, 472, L115
Panov, K.P., Seggewiss, W., 1990, A&A, 227, 117
Poe, C.H., Friend, D.B., Cassinelli, J.P., 1989, ApJ, 337, 888
Prinja, R.K., Massa, D., Fullerton, A.W., 1995, ApJ, 452, L61
Robert, C., Moffat, A.F.J., Bastien, P., Drissen, L., St.-Louis, N., 1989, ApJ, 347, 1034
Robert, C., Moffat, A.F.J., Bastien, P., St.-Louis, N., Drissen, L., 1990, ApJ, 359, 211
Schmidt, G.D., 1998, in 'Polarized Radiation of Circumstellar Origin', G.V. Coyne, A.M. Magalhães, A.F.J. Moffat, R.E. Schulte-Ladbeck, S. Tapia, D.T. Wickramasinghe (eds), U. Arizona, p. 641
Schulte-Ladbeck, R.E., Nordsieck, K.H., Taylor, M., Nook, M.A., Bjorkman, K.S., Magalhães, Anderson C., 1991, ApJ, 382, 301
Schulte-Ladbeck, R.E., Nordsieck, K.H., Taylor, M., Bjorkman, K.S., Magalhães, A.M., Wolff, M.J., 1992, ApJ, 387, 347
Schulte-Ladbeck, R.E., 1994, in 'Instability and Variability of Hot-Star Winds', A.F.J. Moffat, S.P. Owocki, A.W. Fullerton, N. St-Louis (eds), Kluwer (Dordrecht), p.347
Shortridge, K., Meyerdierks, H., Currie, M., Clayton, M., 1996, Starlink User Note, No. 86
Smith, L.F., Shara, M.M., Moffat, A.F.J., 1990, ApJ, 358, 229
Smith, L.F., Shara, M.M., Moffat, A.F.J., 1996, MNRAS, 281, 163
Stahl, O., et al., 1996, A&A, 312, 539
St.-Louis, N., Drissen, L., Moffat, A.F.J., Bastien, P., 1987, ApJ, 322, 870
St.-Louis, N., Moffat, A.F.J., Drissen, L., Bastien, P., Robert, C., 1988, ApJ, 330, 286
St.-Louis, N., Dalton, M.J., Marchenko, S.V., Moffat, A.F.J., Willis, A.J., 1996, ApJ, 452, L57
van der Hucht, K.A., Hidayat, B., Admirato, A.G., Supelli, K.R., Doom, C., 1988, A&A, 199, 217
Vreux, J.M., Andrillat, Y., Gosset, E., 1985, A&A, 149, 337
White, R.L., Becker, R.H., 1995, ApJ, 451, 352
Whitney, B.A., Schulte-Ladbeck, R.E., Aspin, C., Meade, M.R., Anderson, C.M., Clayton, G.C., Murison, M.A., Nordsieck, K.H., Nook, M.A., Schutt, R.L., 1989, BAAS, 20, 1013
Williams, P.M., van der Hucht, K.A., Thé, P.S., 1987, QJRAS, 28. 248
Williams, P.M., van der Hucht, K.A., Pollock, A.M.T., Florkowski, D.R., van der Woerd, H., Wamsteker, W.M., 1990, MNRAS, 243, 662
Wright, A.E., Barlow, M.J., 1975, MNRAS, 170, 41